EXPERIMENTAL DETERMINATION OF LONGITUDINAL VORTICAL PERTURBATIONS

N. F. Yurchenko, V. V. Babenko,
and L. F. Kozlov

UDC 532.526.4

The stability diagram of longitudinal vortical perturbations in a boundary layer on concave surfaces is obtained experimentally.

The possibility of predicting the behavior of longitudinal vortical perturbations in a boundary layer is of prime importance for cases of flow over curved surfaces [1], as well as to establish laws governing the generation of turbulence in a developed turbulent flow [2]. Curves of the neutral stability of longitudinal vortices on concave surfaces (Gortler vortices) that are obtained by numerical methods are ambiguous [3]. Moreover, there is no experimental data that could be compared to these results and help clear up present contradictions.

This article is devoted to an experimental determination of criteria of the stability of longitudinal vortical perturbations.

The method of study is based on the notion of experimental construction of a diagram of linear stability of Tollman–Schlichting waves [4]: with a minimum degree of external turbulence, small perturbations of a certain form are introduced in the boundary layer and their development is followed in relation to the wave number and the parameters of the main flow. On the one hand, such parametric perturbation of the boundary layer excludes the effect of uncontrolled factors and nonlinear interaction of the introduced and natural perturbations. On the other hand, it makes it possible to sequentially follow the reaction of the boundary layer to perturbations of a specified scale. Reinforcement of the introduced perturbations and subsequent disruption of ordered motion beginning at a certain value of one of the parameters when the parameters are constant corresponds to crossing of the neutral curve on the stability diagram.

The experiment was conducted on a hydrodynamic stand [4] with a regulated level of turbulence $\varepsilon \approx (0.05\text{-}10\%)$. The boundary layer was formed on the bottom of the working section, which was made in four variants: flat over its entire length of 3 m, and with a concave part with a curvature of $1/R = 1$, 0.25, and 0.08 m^{-1}. In all cases, the distance from the front end to the beginning of the curvature was 0.5 m, while the maximum sag $H = 0.05$ m. The nonuniformity of the velocity distribution along the channel axis (Fig. 1) reaches 20%. Thus, in this experiment, the laws of the development of vortical perturbations could be studied both in the classical formulation [1] and with complicating conditions: an increase in the degree of turbulence and the presence of a longitudinal pressure gradient. Also, for the surface with $R = 1$ we made a curved transparent cover which was positioned equidistant to the working surface so that flow in a channel with a cylindrical section was realized.

In accordance with the method used in [5], longitudinal vortical perturbations were introduced by means of grids placed on the flow surface in the transverse (z) direction. The grids were part of a vortex generator in the form of a vertical plate $5 \cdot 10^{-5}$ m thick with a split front end. Both parts of the front end were curved in a helix. This stimulated twisting of the flow and the formation of pairs of longitudinal vortices between adjacent generators: a region of decelerated flow (peak, $z = 0$) was formed in the wake after the generator in the xy plane, while a region of accelerated flow (trough, $z = \lambda_z/2$) was formed in the middle between adjacent generators. The distance between generators λ_z was varied within the ranges 0.004-0.032 m, with an interval of 0.002 m. We used

Institute of Hydromechanics, Academy of Sciences of the Ukrainian SSR, Kiev. Translated from Inzhenerno-Fizicheskii Zhurnal, Vol. 50, No. 2, pp. 201-207, February, 1986. Original article submitted October 29, 1984.

 0022-0841/86/5002-0140$12.50

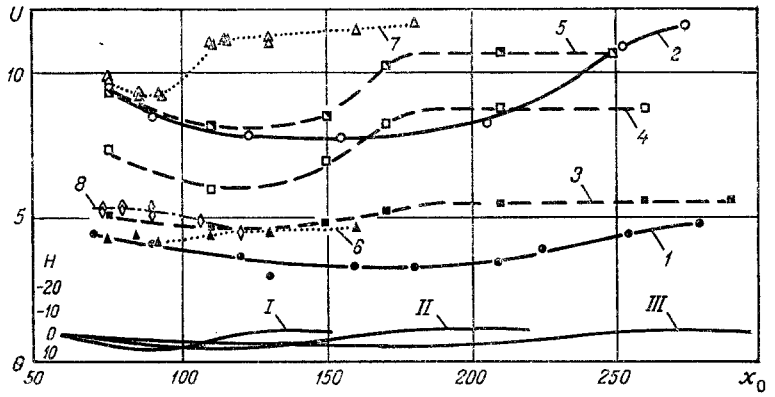

Fig. 1. Profiles of concave sections of a curved bottom with radii of curvature R = 1 m (I), 4 m (II), and 12 m (III), and the velocity distribution along the bottom U_∞ for III (1, 2), II (3-5), and I (6, 7) and the cylindrical surface (8). U, cm/sec; H, x_0, cm.

TABLE 1. Parameters Characterizing Conditions for Determination of Neutral Perturbations

Serial no.	R, m	U_∞, m/sec	x, m	$\lambda_z \cdot 10^2$, m	$\bar{\delta}_2 \cdot 10^3$, m	$\alpha_z \bar{\delta}_2$	G
1	12	0,03	0,6	2,4	2,8	0,73	1,5
2	12	0,035	0,73	2,4	3,5	0,92	2,1
3	12	0,03	2,2	4	1,2	0,18	0,36
4	12	0,08	2,2	2,4	1,45	0,38	1,48
5	4	0,03	1,8	1,6	1,3	0,5	0,84
6	4	0,03	1,8	3,2	1,3	0,25	0,84
7	4	0,05	2,1	1,2	1,5	0,78	1,45
8	4	0,05	2,1	2,4	1,5	0,39	1,45
9	4	0,128	1,8	1,6	1,1	0,43	2,4
10	1	0,087	1,35	1,2	1,75	0,92	6,3

generators of four different sizes: B1 – 0.003 m higher and 0.012 m long; B2 – 0.005 and 0.015 m, respectively; B3 – 0.007 and 0.018 m; B4 – 0.015 and 0.018 m, respectively. In each specific case, the size of the generator was chosen in accordance with the parameters of the main flow and boundary layer and the wavelength λ_z of the introduced perturbations [5].

The kinematic structure of the boundary layer was recorded by photographing the flow field, which was visualized by the electrochemical Teller method. The characteristics were checked with a laser anemometer [6]. Visualization of the velocity profiles U(z) downstream of the grids gave a clear representation of decay and intensification of perturbations with specified parameters. The reliability of the results was ascertained as follows. Two methods were used to detect perturbations with a zero gain, characterized on the stability diagram by points on the neutral curve with the coordinates $G = U_\infty \delta_2^{1,5} \nu^{-1} R^{-0,5} \sim x^{0,75} U_\infty^{0,25} R^{-0,5}$ and $\alpha_z \delta_2 \sim x^{0,5} U_\infty^{-0,5} \lambda_z^{-1}$. A change in λ_z with fixed values of the remaining parameters means a change in the parameter $\alpha_z \delta_2$ and is reflected in shifting of the control point on the stability diagram along the x axis. Observation of the flow field along the working section (along x) with U_∞, R, λ_z = const signifies shifting of the control point along the lines $P = U_\infty \lambda_z^{1,5} \nu^{-1} R^{-0,5} = \text{const}$. The intersection of these curves with the neutral curve on the Gortler diagram corresponds to the formation in the boundary layer of the wavy profile U(z) which is most stable in space and time. Repetition of the procedure for surfaces with different curvatures 1/R makes it possible to cover nearly the entire range of values of G and $\alpha_z \delta_2$ that is of interest.

Table 1 shows the values of the parameters used in experimental determination of points of the neutral curve of the stability diagram.

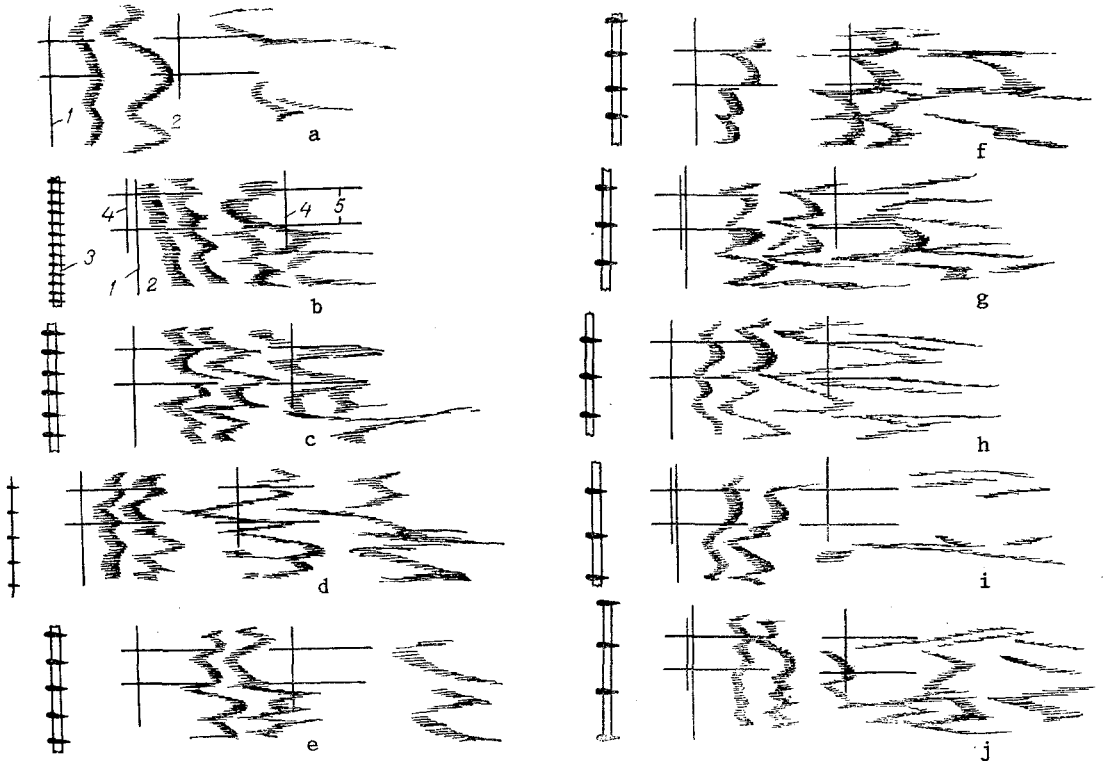

Fig. 2. Selectivity of the reaction of the boundary layer to introduced perturbations (R = 4 m, U_∞ = 0.05 m/sec, x = 2.1 m, y = 0.002 m): a) without the introduction of perturbations; b-j) with the introduction of perturbations with λ_z = 0.008 m (b); 0.012 m (c); 0.016 m (d); 0.018 m (e); 0.02 m (f); 0.022 m (g); 0.024 m (h); 0.026 m (i); 0.028 m (j). (1 – Teller wire; 2 – Teller clouds; 3 – vortex generators; 4, 5) – transverse and longitudinal marks on the bottom of the working section; there is 0.5 m between transverse marks and 0.1 m between longitudinal marks).

Using graphic reproductions of the visualized profiles U(z), Fig. 2 illustrates the selective character of the reaction of the boundary layer in relation to the magnitude λ_z of the introduced perturbations with G = 1.45 and a distance Δx = 0.05 m from the grid of the vortex generator to the Teller wire (this distance was kept constant during the entire experiment).

It turned out that the introduction of perturbations with λ_z = 0.008 m leads not to their decay – as might be expected from the Gortler diagram – but to their transformation into an enlarged structure with $\lambda_z \approx$ 0.016 m (b). Evidently, under these conditions the boundary layer is so sensitive that any disturbance of it causes a reaction. The smallest scale of perturbations at which an adequate reaction is seen corresponds to λ_z = 0.012 m (c), which should be close to neutral perturbations. A further increase in wavelength gives even clearer wave patterns with respect to z (d, e). The tendency toward the formation of a rolled-up vortex sheet (f-h) is evidence of acceleration of the perturbing motion. Beginning with λ_z = 0.024 m, this acceleration stops: the amplitude of U(z) decreases and there is some refinements of the structure compared to the introduced structure (i, j). It can be concluded from this that a vortex system with λ_z = 0.024 m develops with the maximum amount of intensification. An increase in λ_z from 0.012 to 0.024 m is reflected on the Gortler diagram by shifting of the control point to the left. Here, it intersects several curves of equal intensification $\beta^* = \beta\delta_2/\nu$ with increasing values of β. The recorded maximum reinforcement corresponds to the existence of an extremum (minimum) on the curves, which in turn is evidence of the loop-shaped form of the sought neutral curve. The closed character of the instability region also follows from simple physical considerations: large vortex systems cannot grow without limit boundary layer, i.e., the quantity α_z must have a lower bound.

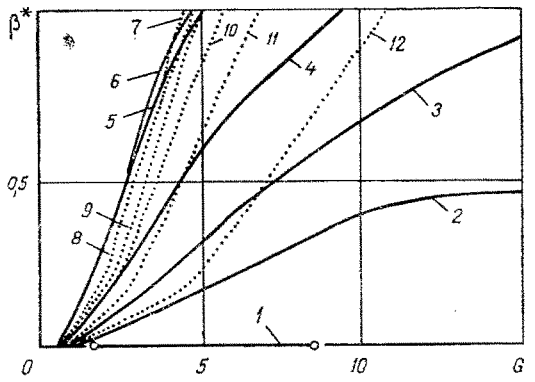

Fig. 3. Gortler stability diagram in the coordinates $\beta^*(G)$ with a change in the wave parameter P: 1) P = 49; 2) 54; 3) 63; 4) 78.7; 5) 126; 6) 157; 7) 236; 8) 315; 9) 472; 10) 787; 11) 1575; 12) 7875.

Measurement of vertical profiles of the longitudinal component of velocity by the laser anemometer confirmed the above conclusions. Only in the case of adequacy of the introduced vortex systems and those developed downstream do we have the characteristic form of the profiles measured at $z = 0$, $z = \lambda_z/4$, and $z = \lambda_z/2$: respectively, with an inflection point near the wall, with an inflection point in the middle part of the boundary layer, and very full profiles without inflection points. Rapid growth of the perturbations makes these features more prominent and increases the amplitude of the visualized profiles U(z).

Construction of the lower branch of the neutral curve is of particular complexity and interest (in connection with the largest differences between the theoretical results). It requires analysis of the development of large-scale perturbations above surfaces with a small curvature exposed to a low-velocity flow. Such analysis entails technical difficulties in organizing these perturbations and is associated with an increase in the measurement error due to small gradients of the gain β with change in any of the dependent variables. In connection with this, first we analyzed the theoretical Gortler stability diagram replotted in the coordinates $\beta^*(G)$ for a broad range of values of the wave parameter P (Fig. 3). The greatest intensification is evidently characterized by perturbations with $P \approx 110\text{-}250$. This is particularly true of small G, but at the same time it is difficult to distinguish the preferred λ_z in this case. However, if we examine the natural development of perturbations in the boundary layer, we can always pick out a specific value of λ_z which to all appearances corresponds to three-dimensional perturbations with the largest gain. The relationship between the gravitational F_1 and centrifugal F_2 forces in a flow on a concave wall $F_1/F_2 \sim U^2/Rg$ reflects the same conditions of development of vortical perturbations on surfaces of different curvature. In fact, the observed value of λ_z of natural perturbations on all four types of surfaces studied fluctuates within the range $\lambda_z = 0.04\text{-}0.05$ m under identical flow conditions, which is in the above-noted region P = 110-250. Here, the value of λ_z was close to the upper limit of the range on the flat surface, while in the flow with a cylindrical section it was close to the lower limit (no flow features affecting the Gortler stability were discovered in the remaining tests in the second case). In connection with the foregoing, it can be concluded that the abscissa of the minimum of the neutral curve will be $\alpha_z\delta_2 \approx 0.13$. Here, δ_2 is determined from conditions on the flat surface exposed to the flow ($\delta_2 \approx 1\cdot10^{-3}$ m).

Also, the minimum point of the neutral curve should be located at the point of its intersection with the curve of maximum intensification. Figure 4 shows an experimental neutral curve and curve of maximum intensification. The lower part of the neutral curve is extrapolated in accordance with the similitude of the form of equal-intensification curves (the closure or loop shape of the instability region) and the above-noted physical mechanism of the development of perturbations. The upper part of the neutral curve is extrapolated from the results of experiments in air conducted by Japanese investigators and described in [7].

The curves obtained here are to the right of the theoretical curves on the diagram, i.e., in an actual boundary layer there is an increase in three-dimensional perturbations with a smaller scale λ_z than predicted by the theory. This is consistent with the result of

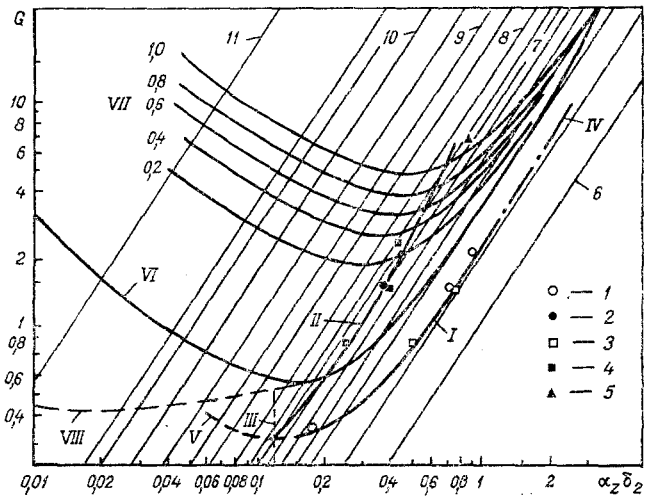

Fig. 4. Stability diagram of longitudinal vortical perturbations on concave surfaces (Gortler). Experimental data: I) neutral curve (1, 3 – points obtained on the surfaces with R = 12 and 4 m); II) curve of maximum intensification (2, 4, 5 – points obtained for R = 12, 4, and 1 mm, respectively); III) line of the critical value $\alpha_z\delta_2 = 0.12$ ($R \to \infty$); IV) experimental results from [7]; V) extrapolation of I; VI, VII) neutral curve and curves of equal intensification according to Gortler's calculations [8]; VIII) theoretical neutral curve of Smith [9]; 6-11) lines of equal values of P: 6) P = 15.75; 7) 94.5; 8) 157.5; 9) 315; 10) 787.5; 11) 7875.

comparison of the experimental and theoretical curves of neutral intensification of Tollman–Schlichting waves in the linear region of their development. This deviation can be attributed to the different degrees of turbulence of the external flow in the experiments ($\varepsilon > 0.1\%$) and calculations ($\varepsilon \leq 0.05\%$).

NOTATION

x, y, z, coordinate axes; g, acceleration due to gravity; U_∞, free flow velocity; U, longitudinal component of velocity on the boundary layer; R, radius of curvature of the surface; Re, Reynolds number along the length; G, Gortler number; P, wave parameter; F_1 and F_2, gravitational and centrifugal forces, respectively; δ_2, momentum thickness; λ_z, wavelength of three-dimensional perturbations with respect to z; ν, kinematic viscosity.

LITERATURE CITED

1. G. Shchlichting, Boundary Layer Theory, McGraw-Hill (1968).
2. R. F. Blackwelder, "Analogies between transitional and turbulent boundary layers," Phys. Fluids, 26, No. 10, 2807-2816 (1983).
3. T. Herbert, "On the stability of the boundary layer along a concave wall," Arch. Mech. Stosow., 28, No. 5-6, 1039-1055 (1976).
4. L. F. Kozlov and V. V. Babenko, Experimental Studies of Boundary Layers [in Russian], Naukova Dumka, Kiev (1978).
5. N. F. Yurchenko, "Method of experimentally studying a system of longitudinal vortices in a boundary layer," Inzh.-Fiz. Zh., 41, No. 6, 966-1002 (1981).
6. V. V. Babenko, V. P. Ivanov, and N. F. Yurchenko, "Measurement of the susceptibility of a boundary layer to planar and three-dimensional perturbations with the aid of a laser anemometer," Avtometriya, No. 3, 91-96 (1982).
7. J. M. Floryan and W. S. Saric, "Stability of Gortler vortices in boundary layers," AIAA J., 10, No. 3, 316-324 (1982).
8. H. Gortler and V. Velte, "Recent mathematical treatment of laminar flow and transitional problems," Phys. Fluids, 10, 3-10 (1967).

9. A. M. O. Smith, "On the growth of Taylor–Gortler vortices along highly concave walls," Q. Appl. Math., 13, No. 3, 233-262 (1955).

EXPERIMENTAL STUDY OF NONSTEADY HEAT CONVECTION IN A PLANE CHANNEL

G. A. Dreitser and V. V. Balashov

UDC 536.24

Results are presented from an experimental study of the effect of thermal and hydrodynamic transience on convective heat transfer in a short plane channel.

Nonsteady thermal processes play a significant and in several cases determining role in modern power plants and manufacturing facilities. To reliably calculate these processes, it is necessary to know the laws governing nonsteady heat convection for different laws of change in the boundary conditions and for different channel cross sections. Several studies [1, 2] have examined processes in circular tubes in detail. Here we perform a special investigation of nonsteady heat transfer in plane channels.

As is known, nonsteady problems of convective heat transfer should be examined as coupled problems [2]. However, such problems cannot be solved theoretically due to the lack of data on the distribution of the turbulent coefficient of momentum transfer and turbulent heat-transfer coefficient across the channel.

Experimental study of coupled problems makes sense only to check specific solutions, since it is impracticable to generalize such experiments due to the effect of additional parameters. Thus, engineering methods of calculation are presently constructed with the use of a unidimensional description of processes in the heat carrier. Here, a local heat-transfer coefficient is employed

$$\alpha(x, \tau) = \frac{q_w(x, \tau)}{T_w(x, \tau) - T_b(x, \tau)}, \tag{1}$$

and it is dependent on the nonsteady boundary conditions.

It has been shown in several theoretical and experimental studies of nonsteady heat transfer that the heat-transfer coefficients found under variable thermal loads and heat-carrier flow rates may differ appreciably from the coefficients calculated from quasisteady relations [1, 2]. With a turbulent flow regime, the effect of thermal and hydrodynamic transience on the relationship between the nonsteady and quasisteady heat-transfer coefficients is expressed in the form of the equation

$$K = \frac{\mathrm{Nu}}{\mathrm{Nu}_s} = f\left(K_{Tg}^*, K_G, \mathrm{Re}, \frac{T_w}{T_b}, \frac{x}{d_e}\right), \tag{2}$$

where

$$K_{Tg}^* = \frac{\partial T_w}{\partial \tau} \frac{1}{T_w} \sqrt{\frac{\lambda_b F}{c_p g G}} \tag{3}$$

and

$$K_G = \frac{\partial G}{\partial \tau} \frac{d_e^2}{G \nu_b} \tag{4}$$

Sero Ordzhonikidze Moscow Aviation Institute. Translated from Inzhenerno-Fizicheskii Zhurnal, Vol. 50, No. 2, pp. 207-214, February, 1986. Original article submitted December 25, 1984.

0022-0841/86/5002-0145$12.50